Experimental Observations of U/Th Decays in Glass

SNO-STR-96-063

W. Frati & R.G. Van de Water

Dec 5 1996

1 Introduction

The following report discusses the results of experiments at the University of Pennsylvania to measure the $\beta\gamma$ decay products of Uranium and Thorium decays in glass. The motivations for this important measurement are discussed at length in the thesis by D. Haslip [1], especially Chapter 6, which is most relevant to the measurements discussed here. To summarize, a handle on PMT $\beta\gamma$ events exists because a significant fraction of them can produce large amount of charge, greater than 5 to 10 photoelectrons, from the β Cherenkov radiating in the glass of the PMT photocathode. Within the SNO detector this results in a large charge measurement in one tube and a overall low Nhit trigger, which is unique to PMT $\beta\gamma$ events. Thus, an overall estimate of this background, and its contribution to the lower regions of the Nhit spectrum, can be determined. However, one piece of information is required, and that is the branching ratio for U/Th decays in PMT glass to produce large charge pulses over some predetermined threshold, such as 5 photoelectrons. A determination of this branching ratio can be made from Monte Carlo studies and has already been reported in [1]. However, to gain confidence in this analysis the branching ratio must be experimentally measured with SNO tubes. This report does not make a measurement of this branching fraction because of the cosmic ray background limitation. However, the decays of U/Th are observed in doped glass, demonstrating that these decays are in principle observable, and that further work to reduce the various sources of background will allow their observation in a SNO PMT. Also measured were energy spectra from two different beta decay sources, which demonstrated that energetic electrons traversing the glass of a PMT can deposit large amounts of charge.

It should be noted that the experiments described here are somewhat different from those reported at the December 1995 SNO collaboration meeting. Those previous experiments were aimed at directly observing PMT $\beta\gamma$ events in a SNO tube. Cosmic rays, however, can produce large amounts of charge in a phototube, mimicking the PMT $\beta\gamma$ signal. Thus, the evidence was not conclusive. The following experiment trys not to be so ambitious, and settles for observing $\beta\gamma$ events in U/Th doped glass, giving us a ball park estimate of the detection efficiency for PMT $\beta\gamma$ events in glass.

2 Experimental Setup

The experimental setup is shown in Figure 1. It consists of six 20cm diameter Hamamatsu SNO tubes arranged on two layers. The bottom layer is the measurement area and consists of four SNO tubes. One tube is in the middle of the area, labeled Q2, facing the three other tubes, labeled T1, Q1, and T2, which are 40cm away (measured from the face of the glass). These three tubes are optically isolated from one other, but can all see Q2. The two tubes, T1 and T2, form the trigger while Q1 is the charge observing tube. Sitting 30 cm above the measurement tubes is the top layer Cosmic Ray Detector (CRD). This is a large square 90x90x1cm^3 sheet of scintillator material which is optically isolated from the bottom layer. At either end of the sheet are two SNO tubes, labeled V1 and V2, looking down at a 45^0 angle at the scintillator sheets. When a cosmic ray/shower passes through the scintillator, the light is detected by one or both of these tubes, allowing a veto of this type of event.

The electronics and DAQ components used to measure and store the relevant physics quantities are SNO prototype systems, thus the sensitive physics measurements made here serve the added purpose of long term system tests. A detailed description of these components can be found in [2][3]. The four tubes V1, V2, Q1 and Q2 are attached to the SNO prototype high voltage card (HVC) and eight channel front end card (pFEC), where their charge and time measurements are recorded and stored in local memory. The voltage supplied to all the tubes by the HVC is 2000 Volts. The trigger tubes, T1 and T2, are fed to NIM discriminators, outputting 50 nsec NIM signals going to a NIM coincidence circuit. This trigger signal is supplied to the pFEC and determines when an event is recorded. The information from one or more of the tubes Q1, Q2, V1 and V2 firing within a 250 nsec interval during a trigger pulse, is saved into the pFEC memory. The quantities saved for each fired tube are the measured charge (low and high gain), the time relative to the trigger, and various digital data which are used for CMOS cell identification and event building.

A typical data run lasted about 24 hours, and once completed the data in the pFEC memory is moved to the DAQ computer (Quadra 950) using the U. Washington/Penn code. This data is then moved to a SUN workstation, via ftp, for analysis using SNOLIB/SNOREAD code. Various offline programs have been written at Penn to

build the multi-tube events, reformat the raw DAQ data into ZDAB banks, reduce calibration data into electronic pedestals/calibration, and analyze the data runs. It should be noted that all these programs are linked against SNOLIB, thus maintaining the SNOMAN data structure conventions. Thus many of these programs can serve as a basis for the analysis of real SNO data.

3 Calibrations

The SNO tubes were calibrated using a low intensity light source (beta emitter plus acrylic). The single photoelectron spectrum was acquired for each tube and the number of ADC counts per photoelectron was calculated. Figure 2 shows the single PE distribution of Q1 for a single CMOS cell, which has a zero charge point (pedestal) at -2510.1+/-0.5 counts.

The threshold was set to remove most of the electronic noise events that populate the pedestal region. This threshold corresponds to about 0.25 pe. The difference between the mean of the distribution and the pedestal was taken as the definition of 1.0 pe. Subtracting the pedestal from the data for all 16 CMOS cells, and then adding these distributions together, yields a mean calibration of 4.95 counts/pe (this will be about 20 counts/pe for the production electronics). This is an overestimate since the threshold cut is removing some of the events at lower charge.

Another definition of the single pe calibration is to take the difference between the pedestal and single photoelectron peak, which corresponds to about 4 counts/pe. From this we estimate 20% as the systematic error on the charge calibrations of 4.95 counts/pe for tube Q1. The ratio between the high and low gain charge channels is 4 to 1. The remaining tubes were calibrated in a similar fashion. The noise rates for all the tubes were around 3 kHz. The pedestals, calibrations and noise rates for each channel was monitored periodically to ensure stability.

The TAC for each channel was calibrated using a precision pulser which fed the pedestal and Global Trigger (GT) pulses into the pFEC. The TAC calibration was found to be -2.4 TAC counts per nanosecond. Since precise TAC measurements are not necessary for this analysis, the small difference between the two QNSN7 internal TACs per channel was ignored.

The data subsequently shown in this report have been pedestal subtracted with all CMOS channels added together, and are calibrated with charge expressed in units of photoelectrons (pe), and TAC time in nanoseconds (nsec).

4 Results and Analysis

4.1 Backgrounds

Before presenting the results of the calibration sources and U/Th doped glass measurements a discussion of the primary source of background is in order. Cosmic rays are the most abundant and annoying source of radiation in this experiment. This is attributed to the fact that they come from all directions and that they can produce large amounts of Cherenkov light when traversing the glass of a PMT. In fact, it has been reported [4] that high energy cosmic rays and showers can produce as much as hundreds of photoelectrons in a PMT, though most events produce only a few photoelectrons. The point is that the deposited energy spectrum extends over a large region, including the region where we expect to see PMT $\beta\gamma$ events.

Figure 3 shows the Q2 charge versus TAC time during a data run when the Q2 tube is optically uncovered, i.e. visible to Q1 and the two trigger tubes. Most of the triggers occurring are cosmic rays passing through Q2, producing a large charge deposit there, and at the same time some photons escape to hit the trigger tubes T1 and T2. The first thing to notice is that there are a large number of events at TAC time between 100 and 135 nsec with large charge deposits. These correspond to in-time events which trigger Q2, T1 and T2 simultaneously, such as cosmic rays and other background radiation. The 100 nsec corresponds to cable and gate delays. The clumping of large charge events at early times from 150 to 175 nanoseconds (note, large TAC times corresponds to early PMT hits) are energetic photons or charged particles striking the first dynode of Q2 directly. The time between this clumping and the in-time events corresponds to the drift time for electrons between the photo cathode and the first dynode. The low charge events from 0 to 100 nanoseconds are out of time random triggers. Thus, the physics events of interest are the in-time events in the TAC window from 90 to 140 nanoseconds. All the subsequent plots of charge will have this TAC selection applied.

Figure 4 shows the charge distributions for Q1 and Q2 with the requirement that V1 or V2 fired, henceforth, defined as the cosmic ray detector on (CRD-ON), implying a cosmic ray is present. Also displayed in Figure 4 are the charge distributions for Q1 and Q2 with the cosmic ray detector off (CRD-OFF), i.e. neither V1 or V2 fired. With CRD-ON, the charge distribution extends out to hundreds of photoelectrons, as expected. With CRD-OFF, the rate suppression is significant, but a number of cosmic rays still leak through, especially at low values of charge. This happens because the solid angle subtended by the CRD is only 50%. However, folding this with the flux angular distribution, it is estimated that 87% of the cosmic rays are rejected for the situation when all four tubes, Q1, Q2, T1 and T2 fire. These undetected cosmic rays enter the detector from the sides, and are traveling in a horizontal direction. Because Q1 is at the edge of the the CRD coverage, more high energy cosmic rays leak through, hence the observed higher charge distribution in this tube relative to Q2.

4.2 Calibration Sources

To determine the shape and extent of the charge distribution from low energy β rays traversing the SNO PMT glass, two different sources with β energies similar to U/Th decays were used. The first was ^{109}Ru with a primary β^- end point energy of 3.5 MeV, and the second source was ^{90}Sr with a primary β^- end point energy of 2.3 MeV. These sources were individually placed next to the photocathode glass of Q2, ensuring that most of their energy was deposited in the glass and not in the air.

The data for these calibration runs are shown in Figure 5, where the charge distributions observed in Q1 and Q2 are displayed for each of the sources. The Q2 data is for the triple coincidence of Q2, T1 and T2, while the Q1 data is for the quadruple coincidence of Q1, Q2, T1 and T2. Both require CRD-OFF, these triggers are interpreted as the β^- striking the glass of Q2, and the subsequent Cherenkov light hitting Q1, T1 and T2. The first characteristic to note is that there are few cosmic rays, denoted by the small number of large pulse height events, since the activity of the sources are much higher than the cosmic ray rate. The Q2 distribution shows that most events produce less than 50 photoelectrons of deposited energy, peaking around 9 pe and 6 pe for the ^{109}Ru and ^{90}Sr sources, respectively. From this it is estimated that on

average 1 MeV of β energy deposits about 3 to 4 photoelectrons of detectable light in the PMT glass, and can fluctuate up to a maximum of 17 photoelectrons per MeV.

The above calibrations are to be taken as upper limits since we require a coincidence of three external tubes, which has a greater efficiency for large Q events. Looking at the differences in the mean of Q2 for three and four fold coincidences, it is estimated that the above calibrations should be reduced by 30%. The experimental charge calibration distributions for Q2 should be compared to the SNOMAN calculation for PMT $\beta\gamma$ events, which are shown in Figure 6. Though the shapes are different, the endpoint of the ^{109}Ru and the SNOMAN distributions are roughly equivalent at 40 to 50 photoelectrons, after falling three decades, giving us some confidence in the PMT simulation and measurements. The small differences in shape can be attributed to the fact that the calibration sources are dominated by a single β, while real PMT $\beta\gamma$ events consists of many more decay chains involving lower energy β's and energetic γ rays.

The charge in the observing tube Q1 is consistent with low photoelectrons multiplicity. This is to be expected since the probability of Cherenkov photons produced in Q2 escaping the glass and producing a photoelectron in Q1 is low. However, it does demonstrate that some fraction of Cherenkov photons do indeed escape the source tube Q2 and can trigger observing tubes Q1, T1 and T2. An estimate of this probability is given by the ratio of the threefold coincidence rate excluding Q1, to the fourfold coincidence rate including Q1. It is observed to be about 0.07, which as expected is small but still significant. Removing the solid angle effects, it is estimated that up to 20% of the Cherenkov photons can escape the source tube.

4.3 U/Th Doped Glass

The second set of experiments was to try to observe U/Th decays in glass. This was accomplished by placing a U/Th doped glass plate (kindly made available by Rick Norman at LBL), with dimensions 14.5x13x0.5cm^3, directly in front of Q2 where it just touches the glass of the PMT. Based on activity measurements at LBL (about 0.5ppm), the rate of observable high energy β U/Th decays in the glass is estimated to be around 1.4 Hz. A signal was searched for by looking for an excess of events in the observing tube Q1, with and without the doped glass in place. However, the difficulty

with this simple subtraction analysis is to reject the increase in rate due to the passage of cosmic rays through the doped glass.

The trick here is to now use the Q2 tube as part of the cosmic ray veto. The justification for this comes from the fact that a cosmic ray passing though the doped glass will most likely pass though Q2, or at least produce enough Cherenkov photons with the right geometry to trigger it. Vertical cosmic rays from above are vetoed by the CRD, while horizontal ones, which come in from the sides, remain undetected.

The horizontal events that traverse the doped glass must also pass through the PMT since it has about twice the surface area and is in close proximity to the doped glass. There is only a very small solid angle, directly along the length of the doped glass, where the cosmic rays can pass through without striking the PMT. However, these events are most likely detected since the passing cosmic ray produces a Cherenkov cone that intersects with the PMT. Thus, if we require only a threefold coincidence between Q1, T1 and T2, we reject those horizontal cosmic ray events defined above. At the same time, $\beta\gamma$ events in the doped glass have some directionality, since the β particle radiates in a Cherenkov cone along its path of travel. Therefore, we expect some fraction of these events to radiate only in the forward direction towards Q1, T1 and T2 while simultaneously missing Q2. From simple geometrical arguments this fraction is estimated to be about 25%. The four fold rate, which includes Q2, is expected to be even more reduced, since it is less geometrically favored.

The observed data rates in Q1 for sixteen different experimental trigger and setup conditions are shown in Tables 1 and 2. The rates in both of these tables are averages over many runs, and can represent as much as one to five days of data collection. The two tables are identical except the first one is with CRD-ON, representing the cosmic ray data sample, and the second table is with CRD-OFF, which has a minimum cosmic ray contamination. Each row in both tables correspond to a particular trigger condition. We will use the following nomenclature to described these various trigger conditions,

C = CRD-ON: $\overline{C}$ = CRD-OFF

T = two fold T1 and T2 coincidence trigger

$Q1$= Q1 firing: $\overline{Q1}$= Q1 not firing

$Q2$= Q2 firing: $\overline{Q2}$= Q2 not firing.

The second, third and forth columns in the tables correspond to different setup conditions, the first two are background runs and the third is a signal run. The first background run corresponds to a black cloth draped over Q2, optically isolating it from the other tubes. The second background run is Q2 uncovered and no doped glass, while the signal run has the doped glass placed in front of Q2. The difference between these last two columns, glass in minus glass out, is the sum of the U/Th $\beta\gamma$ signal and the cosmic ray background in the doped glass, which is shown in the fifth column.

The cosmic ray rejection capability of Q2 is demonstrated in Table 1. For the first trigger condition $C \cdot T \cdot Q1 \cdot Q2$, which is assumed to be dominated by vertical cosmic rays, we can see that the rates for Q1 increase when Q2 is uncovered and when the doped glass is placed in front of Q2. This is to be expected since the vertical cosmic rays passing through the extra glass cause more detectable triggers.

The interesting numbers are in the next line which shows the second coincidence situation when Q2 is not part of the trigger, $C \cdot T \cdot Q1 \cdot \overline{Q2}$. Here, the rates remain constant. This implies that indeed Q2 is acting as a cosmic ray veto, since the increase in triggers are caught by Q2 and shows up in the rates for $C \cdot T \cdot Q1 \cdot Q2$. There is a small increase in the glass in minus glass out rate, for the second trigger condition, of 5.1 ± 1.6 N/hrs, which compares with an excess rate of 90.1 ± 3.9 N/hrs for the first trigger condition. This implies that Q2 has an efficiency to reject vertical cosmic rays passing through the doped glass of $\epsilon_{cv} = 90.1/(90.1 + 5.1) = 0.94 \pm 0.02$. We will use this number, along with the assumption that Q2 is equally efficient for vetoing horizontal cosmic rays, to calculate the horizontal component of cosmic rays passing through the doped glass. This last assumption is valid since the geometry of the doped glass placed in front of Q2 is similar in both the vertical and horizontal direction, and should not have any biases for either orientation.

The observed data rates in Q1 with CRD-OFF are shown in Table 2, which corresponds to a data sample with the vertical cosmic ray component mostly removed, leaving only the much smaller horizontal flux and U/Th $\beta\gamma$ decays. The third trigger condition $\overline{C} \cdot T \cdot Q1 \cdot Q2$, shows the expected increase in rate due to cosmic rays as we un-

Trigger	Q2 Covered No Glass	Q2 Uncovered Glass Out	Q2 Uncovered Glass In	(Glass In) -(Glass Out)
$C \cdot T \cdot Q1 \cdot Q2$	112.93.5	152.4 ± 2.2	242.5 ± 3.2	90.1 ± 3.9
$C \cdot T \cdot Q1 \cdot \overline{Q2}$	91.0 ± 1.5	87.3 ± 1.0	92.4 ± 1.3	5.1 ± 1.6

Table 1: Observed in-time rates for Q1 (units of N/hrs) with CRD-ON, i.e. cosmic ray data sample.

Trigger	Q2 Covered No Glass	Q2 Uncovered Glass Out	Q2 Uncovered Glass In	(Glass In) -(Glass Out)
$\overline{C} \cdot T \cdot Q1 \cdot Q2$	1.9 ± 0.1	15.4 ± 1.4	22.0 ± 0.9	6.6 ± 1.7
$\overline{C} \cdot T \cdot Q1 \cdot \overline{Q2}$	56.1 ± 1.2	55.9 ± 0.8	64.7 ± 1.1	8.8 ± 1.4

Table 2: Observed in-time rates for Q1 (units of N/hrs) with CRD-OFF.

cover Q2 and add the doped glass. However, the fourth trigger condition, $\overline{C} \cdot T \cdot Q1 \cdot \overline{Q2}$, shows something different. The rates with and without the cover are the same, while the rate with the doped glass increases, with an excess of 8.8 ± 1.4 N/hr over the glass out background run. This increase in the doped glass is due to U/Th decays and cosmic rays not rejected by Q2. The undetected cosmic ray rate in the glass can be calculated using the Q2 rejection efficiency, estimated above, and the observed horizontal cosmic ray rate for the third trigger condition, giving, $(1 - \epsilon_{cv}) \times 6.6 = 0.4 \pm 0.2$ N/hrs. This is subtracted from the observed signal+background excess, giving a U/Th signal rate in the doped glass of 8.4 ± 1.4 N/hrs. A plot of the excess charge distribution observed in Q1 is shown in Figure 7. The distribution is characteristic of low charge multiplicity, which is anticipated from the calibration runs (compare with Figure 5). The fact that there is minimal to no excess of events at high charge implies that the cosmic ray background has been mostly subtracted out.

Given that the estimated activity of the doped glass is 1.4 Hz, this implies a detection efficiency of our apparatus to observe U/Th decays in glass of $0.17 \pm 0.03\%$.

5 Conclusions and Future Experiments

To summarize, the detected energy spectra of various sources with β energies on the order of a few MeV, similar to those of U/Th decays, has been measured in a SNO PMT. The observed spectrum demonstrates that as much as 50 photoelectrons can be detected in a SNO tube, giving these events a unique topology in the SNO detector. These calibration source measurements were also found to be in reasonable agreement with SNOMAN monte carlo predictions.

The decays of U/Th in a sheet of calibrated glass has been observed, demonstrating in principle that these decays can be observed in SNO PMT's using SNO prototype electronics. With further reduction in the primary source of backgrounds, e.g. cosmic rays, this goal should be achievable. To this end, future work in this area will concentrate on setting up similar experiments in the SNO underground cavity, where cosmic ray rates are negligible. In such an environment, U/Th decays in a SNO tube should be observable. Assuming a "Green Book" U/Th concentration of 30ppb, we then expect a raw event rate of 0.3 Hz in a single SNO PMT. If we now use the Q2 tube as the $\beta\gamma$ source (instead of the doped glass), and assuming the detection efficiency of 0.17% as determined above, we then expect to detect 1.8 events/hour for a four fold coincidence. This is significantly larger than the expected cosmic ray rate.

Another possible experiment is to use a single SNO PMT that is optically isolated and connected to a special setup using SNO production electronics. The tubed is secured to a cable and then dropped into the heavy water where the threshold is set to a high value, such as 5 photoelectrons, and events recorded. Since the heavy water is essentially a radiation free environment, i.e. no cosmics or radioactivity from the cavity wall, any detected events in the PMT are most probably due to U/Th decays in the glass. From Monte Carlo studies the expected PMT $\beta\gamma$ event rate for a 5 pe threshold is estimated to be 40 events/hour, which is significantly larger than the 1.8 event/hour above since we now only require a single tube coincidence. The total activity in the PMT can be determined at a later date by crushing the tube and measuring the U/Th concentration using conventional nuclear techniques. With these two measurements the branching fraction for large charge U/Th decays can be simply estimated since we are free of detection efficiency calculations. The only requirement is a background free

environment, which the SNO heavy water region should provide.

It is important to gain as much information as possible about PMT $\beta\gamma$ decay topologies, rates, etc, in a small scale and controlled experimental situation. Once these individual tube quantities/characteristics are understood, it can then be applied to the detector at large, allowing us to determine the appropriate energy and Nhit thresholds to trigger on this special class of events. With a knowledge of the high threshold branching fraction, then an absolute normalization of the PMT $\beta\gamma$ background in the SNO detector can be determined. This certainly is a measurement worth some effort and resources.

References

[1] An Examination of the PMT $\beta\gamma$ Background in he SNO Detector, by Dean Haslip, Masters Thesis, Queen's University, (1996).

[2] SNO pFEC System Test Results, **SNO-STR-95-010 U.**

[3] The Sudbury Neutrino Observatory electronics Chain, T. Ekenburg et al., submitted to IEEE Transactions of Nuclear Science, Proceedings of the Nuclear Science Symposium, Nov. 1994.

[4] Cosmic Ray Induced Dark Current in Photomultipliers, A.T. Young, Review of Scientific Instruments, Volume 37, Number 11, pg 1472 (1966).

6 Figures

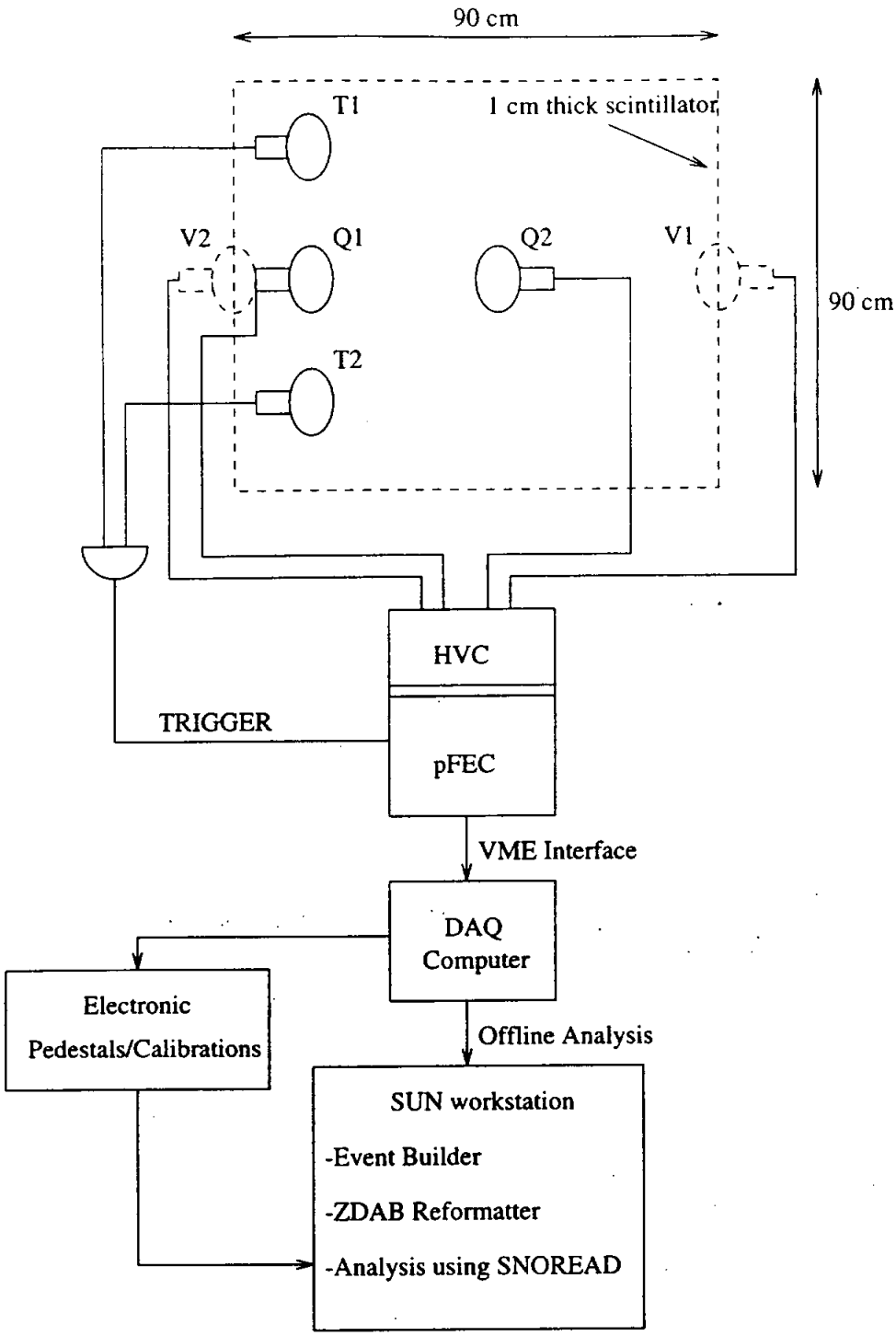

Figure 1: The experimental setup (μSNO-A), and the DAQ/analysis flow diagram. The dotted lines correspond to the top level scintillator and PMT's, which form the Cosmic Ray Detector. The solid line measurement PMT's are 30 cm below on the bottom layer.

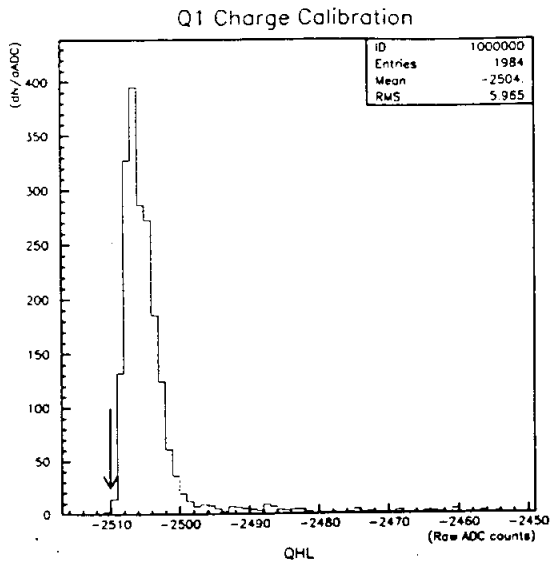

Figure 2: A sample single photoelectron distribution for Q1 with charge threshold of 0.25 pe. The pedestal is at -2510 counts (arrow).

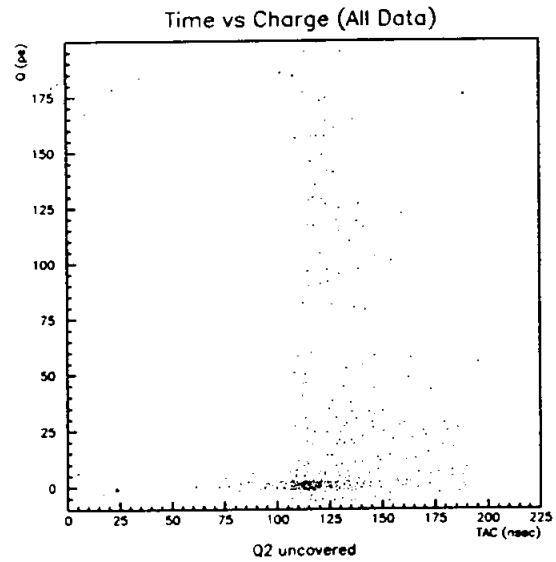

Figure 3: A charge versus TAC scatter plot for Q2 uncovered. Both T1 and T2 fired, no special selection on Q1, V1 and V2.

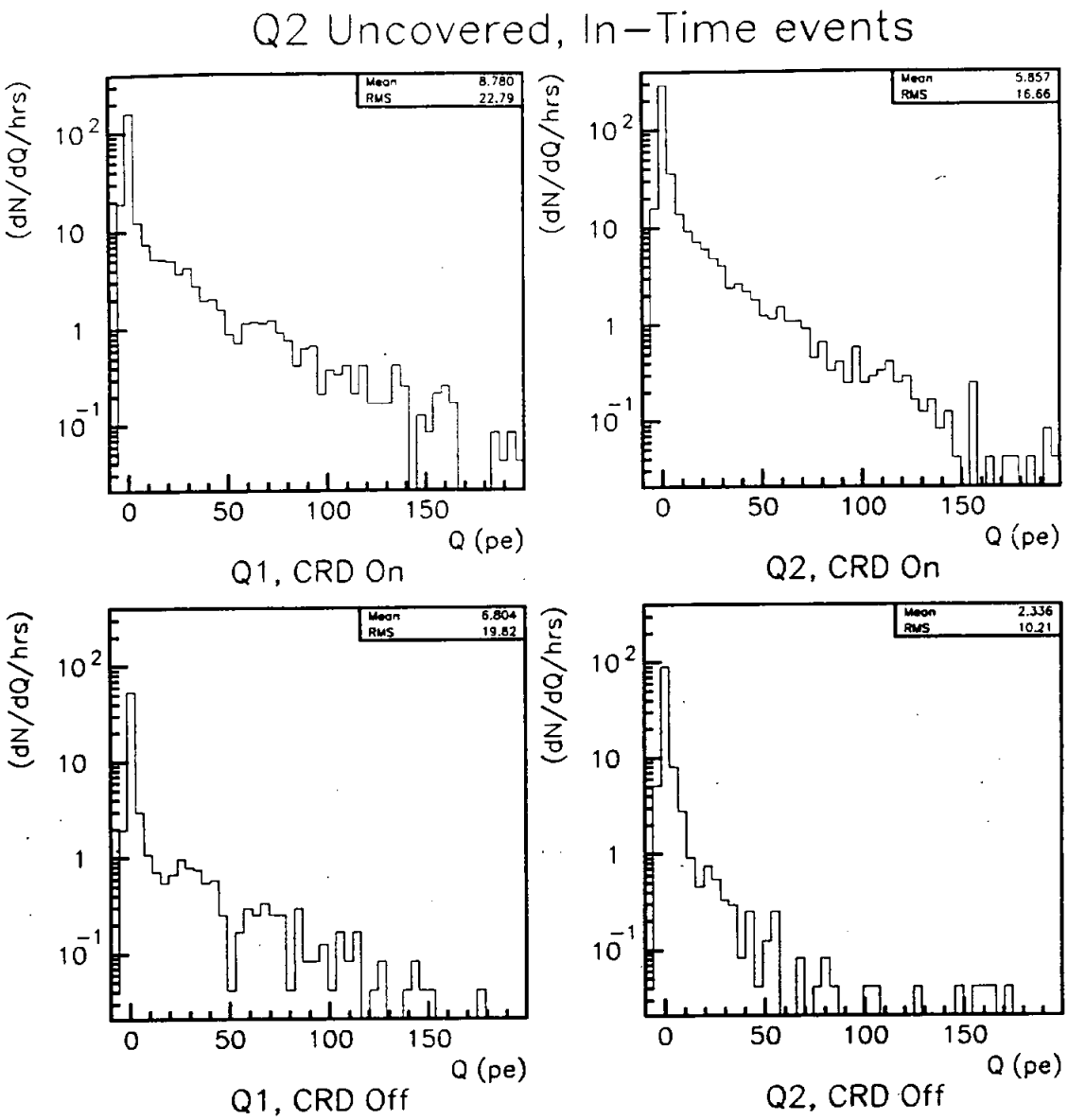

Figure 4: The Q1 and Q2 charge distributions for CRD-ON and CRD-OFF.

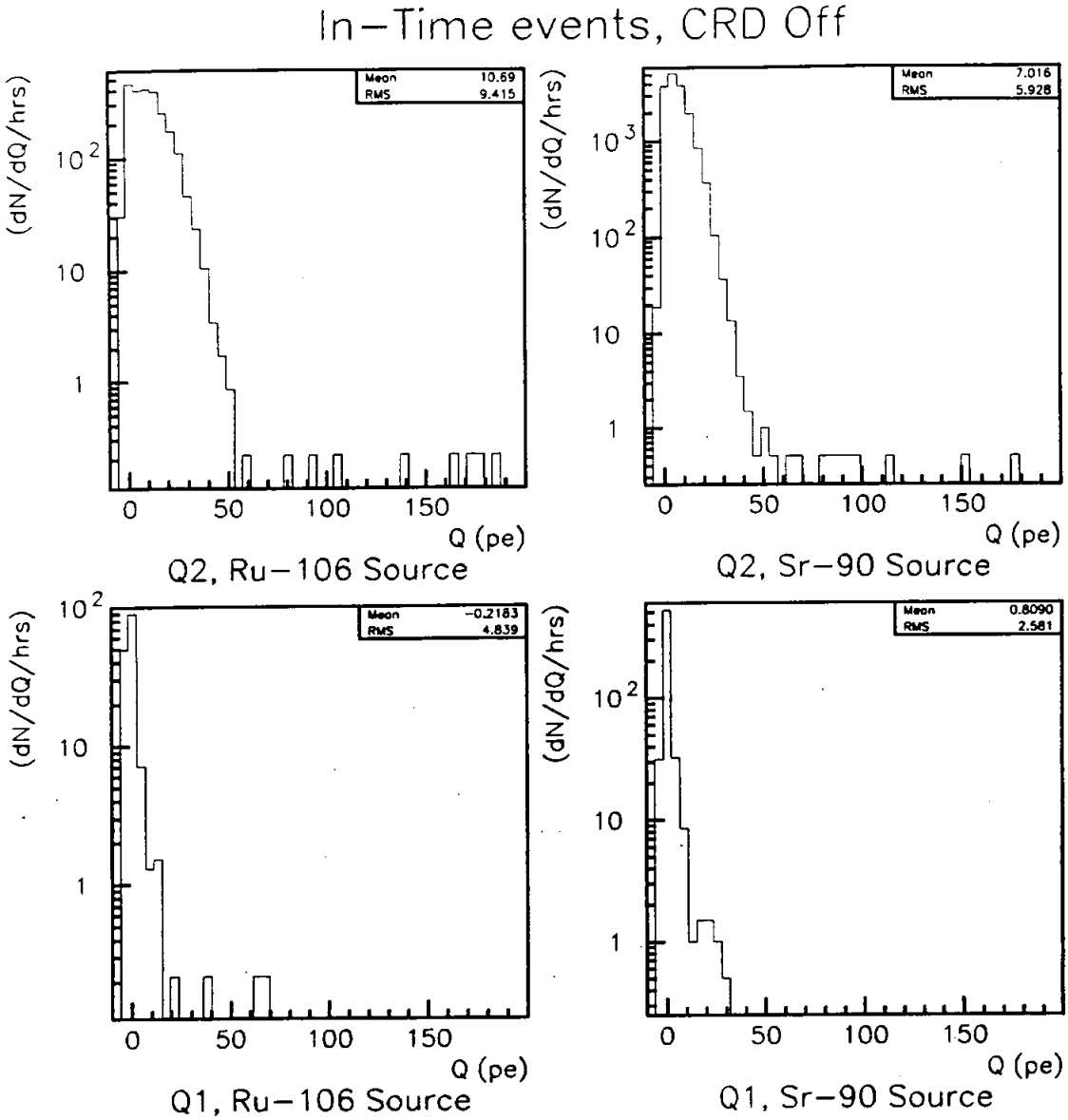

Figure 5: The Q1 and Q2 charge distributions for the ^{109}Ru and ^{90}Sr calibration runs.

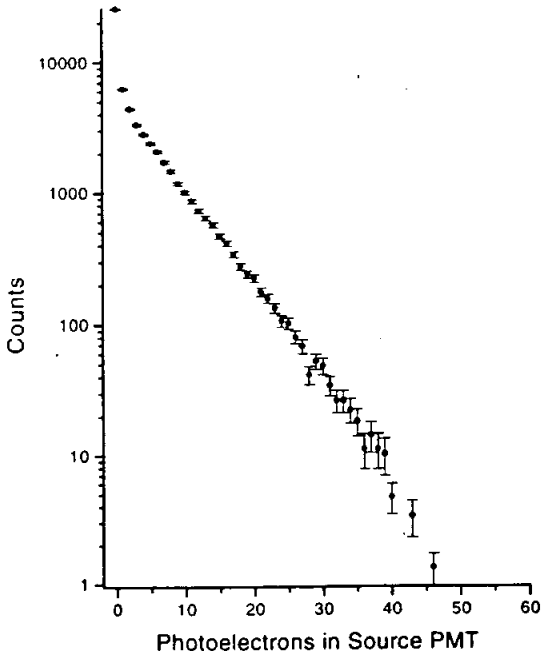

Figure 6: The SNOMAN generated PMT $\beta\gamma$ charge distribution [1].

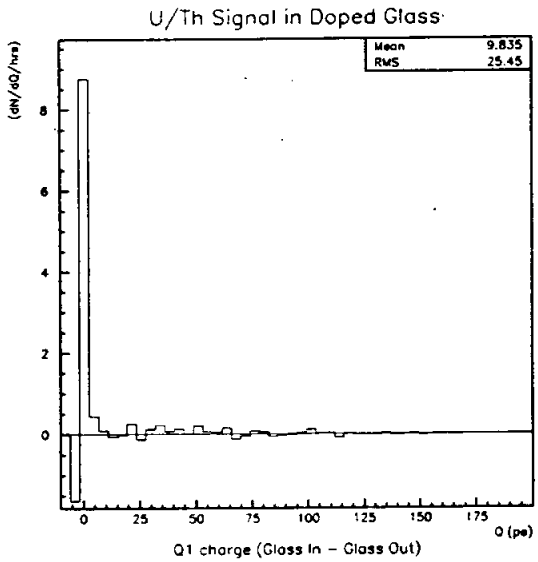

Figure 7: The doped glass excess charge distribution measured by Q1 for the trigger condition $\overline{C} \cdot T \cdot Q1 \cdot \overline{Q2}$.